Report LR-714

Impact tests on Fibre Metal Laminates under a tensile load

March 1993

A. Vlot

TU Delft
Delft University of Technology

Faculty of Aerospace Engineering

Impact tests on Fibre Metal Laminates under a tensile load

A. Vlot

Abstract

The well-known sensitivity of conventional composites to incidental damage such as impact has slowed their widespread application to thin, damage tolerance-critical primary structures such as fuselage pressure cabin skins. Therefore, impact tests were performed to determine the impact characteristics of fibre metal laminates (GLARE and ARALL). Comparative low and high velocity impact tests were performed on monolithic aluminium, fibre metal laminates, and carbon thermoplastic composites. Additional impact tests were performed on monolithic aluminium and ARALL specimens under tensile loading.

GLARE has a larger damaged area than aluminium after ballistic impact of fragment simulating projectiles, but its residual strength was approximately equal.

The results demonstrate the superior behavior of GLARE 3 compared with the other materials. The effect of the initial tensile loading on the damage size and the residual strength of ARALL is small for normal operating stresses ($S < 200$ MPa).

1. Introduction

The family of highly fatigue resistant fibre metal laminates ARALL and GLARE were developed primarily at Delft University over the past decade (Ref.6,10,17,18). The laminates consist of thin high-strength aluminium alloy sheets bonded together with strong fibre/adhesive prepreg. The prepregs are aramid or glass fibres in an epoxy adhesive. The variant with aramid fibres is usually called ARALL. GLARE incorporates glass fibres.

Fibre metal laminates were developed as a material with a high fatigue resistance, achieved by fibre bridging of fatigue cracks and a favourable residual stress system in this hybrid material. If a crack has initiated in the aluminium alloy layers, some limited delamination will occur at the interfaces between the epoxy and the fibres. That will accommodate stress redistribution from the metal to unbroken fibres in the wake of the crack. Crack bridging provided by the strong fibres restrains crack opening, and thus reduces the driving force for crack growth in the metal layers (see Fig.1). Fibre metal laminates combine the formability and machinability of aluminium alloys with the good fatigue resistance and high specific strength of composite materials ('the best of both worlds').

The material can be poststretched. Poststretching causes a reversal of the residual stress system from tensile stresses in the aluminium layers and compressive stresses in the prepreg layers after curing (due to the difference in thermal

expansion coefficients) to compression in the aluminium and tension in the prepreg. The compressive stresses in the aluminium make the fatigue properties of the poststretched material even better than of the as cured material.

The folowing grades are defined:

grade	Al alloy	fibre type	fibre orientation	poststretch
GLARE 1	7475-T76	glass	unidirectional	0.5%
GLARE 2	2024-T3			no
GLARE 3	2024-T3		50/50 cross-ply	no
GLARE 4	2024-T3		67/33 cross-ply	no
ARALL 1	7075-T6	aramid	unidirectional	0.4%
ARALL 2	2024-T3			no
ARALL 3	7475-T76			0.4%

The laminates are applicable in various thicknesses; e.g., a 3/2 lay-up means a laminate with three aluminium layers and two intermediate prepreg layers: [aluminium/prepreg/aluminium/prepreg/aluminium]. As the table above shows, unidirectional and 0/90 cross-plied fibre lay-ups are available. Thus, a wide range of tailorable properties is available to the aircraft designer. ARALL 3 material is currently in production and flight test on the C-17 aft cargo door.

2. Low and high velocity impact tests

2.1 Introduction

The present article characterizes the impact properties of fibre metal laminates in comparison with other high-performance aerospace structural materials.

Impact damage is a relevant damage type for aircraft structures. The analysis of 688 repairs to 71 Boeing 747 fuselages showed that 57% of the repairs involved fatigue damage, 29% were for corrosion and 13% related to impact damage (Ref.18). The actual number of impact damages will be substantially higher, because conventional aluminium alloys are very damage resistant, and the impact damage is only repaired if a crack is present or when the dent depth reaches a prescribed value. This is important for less impact damage resistant materials like composites, for which the number of required repairs may be much higher. The importance of impact damage was also shown by Gökgöl (Ref.4). He monitored 25 cases of impact damage on the tail surfaces of a fleet of 114 Lufthansa aircraft in 14 months.

Impact damage of aircraft structures may be caused by the following sources: runway debris, hail, maintenance damage (dropped tools), collisions between service cars or cargo and the structure, bird strikes, ice from propellers striking the fuselage, engine debris and tire shrapnel from tread separation and tire rupture. Ballistic impact must be added to this list of hazards for military aircraft.

The present section presents results of static indentation and low and high velocity impact tests on ARALL 2, GLARE 3, monolithic aluminium 2024-T3 and carbon/PEEK thermoplastic composites and compares the damage resistance of those materials. The static tests represent collisions of high masses at very low velocities as may be the case for collisions at low velocities of service trucks and cargo containers with the aircraft. The low velocity tests (up to 10 m/s) provide realistic circumstances for maintenance damage (dropped tools). The high impact velocities (up to 100 m/s) are more realistic velocities for runway debris and hail strikes.

2.2 Tested Materials

The following materials were tested:

1. **Monolithic Al 2024-T3.** Bare material was chemically milled from 1.5 to 1.37 mm thickness, to have the same thickness and approximately the same surface density (mass per unit area) as GLARE 3. Clad material was also tested with a thickness of 1.6 mm to represent the baseline material (Airbus A340 fuselage), which could be replaced by GLARE 3.
2. **ARALL 2.** A fibre metal laminate which consists of three layers of 0.3 mm Al 2024-T3 and 2 intermediate unidirectional aramid/epoxy layers with a thickness of 0.2 mm. This 3/2 lay-up can be described as follows:

[Al 2024/UD aramid 0°/Al 2024/UD aramid 0°/Al 2024].

The total thickness was 1.35 mm. No poststretch was applied. ARALL 2 was tested at static loading and low velocity impact only.
3. **GLARE 3.** This fibre metal laminate has a 3/2 lay-up: three 0.3 mm Al 2024-T3 layers and three intermediate layers of glass/epoxy prepreg oriented in two directions. This 3/2 lay-up can be described as follows:

[Al 2024/UD glass 0°/UD glass 90°/Al 2024/UD glass 90°/UD glass 0°/Al 2024].

The total sheet thickness was $h = 1.37$ mm. The material was in the as-cured condition (no poststretch).
4. **Carbon/PEEK composites.** An ICI unidirectional preimpregnated tape was used (APC-2), with an AS4 carbon fibre. The fibre volume fraction of the laminate was 61%. Two lay-ups were tested:
- A cross-ply lay-up [0/90] of 11 plies with a total thickness 1.37 mm (equal to GLARE 3).
- A quasi-isotropic lay-up $[\pm 45/0/90/\pm 45/0/90]_s$ with approximately the same surface density as GLARE 3 and a total thickness of 2.05 mm.

2.3 Test set-up

The specimens with a size of 125x125 mm^2 were clamped between two plates with a square 100x100 mm^2 opening by 8 bolts with a torque of 50 Nm.

The static, low velocity and high velocity tests were performed with a hemispherical steel tip indentor of radius 7.5 mm. The static tests were performed with a loading rate of 1 mm/min. The force-deflection ($F\text{-}w_0$) curve was measured during static loading, and the energy at the first significant load drop (first failure energy U_f) was determined by integration of this curve.

The low velocity impact tests were performed with a drop weight impact tester, with an impactor mass of 575 g (for a detailed description: Ref.18). In a few cases an impactor mass of 2333 g was used (only if explicitly stated). The maximum drop height was 12 m; a maximum velocity in the order of 10 m/s was reached. After impact, the impactor was caught to prevent a second impact.

The high velocity impact tests were performed with a gas gun. After burning through the membrane of the gas gun, the expanding air accelerated a projectile with a mass of 23.3 g up to a maximum velocity of 100 m/s.

The carbon/PEEK specimens were C-scanned, and the delaminated area and the damage width (= diameter of the smallest circle around the delaminated area) was determined. The outer aluminium layers of the GLARE and ARALL specimens were removed by etching to reveal the damage width. These specimens could not be C-scanned because the plastically deformed dent reflected the ultrasonic waves.

2.4 Results

Damage width

The damage width of GLARE 3 and carbon/PEEK is illustrated in Fig. 2. GLARE 3 has a smaller delaminated region than carbon/PEEK. There is no difference between the damage width of GLARE 3 for high and low velocity impact loading.

In Fig.3 the remarkable difference in damage resistance of GLARE 3, monolithic aluminium and carbon/PEEK at 100 J (high velocity) is illustrated. At this energy level only GLARE 3 does not have a perforation and only a minor crack. Fatigue and residual tensile tests showed that GLARE with those small cracks retain their excellent fatigue properties and that the residual strength is hardly influenced.

Minimum cracking energy

A comparison between the minimum cracking energy U_f for materials with approximately equal surface density and a comparison between GLARE 3 and the Al 2024-T3, $h = 1.6$ mm baseline fuselage material is made in Fig. 4. For an equal areal density the minimum cracking energy of GLARE 3 is superior to Al 2024-T3 and carbon/PEEK for static and dynamic loading.

For static loading, the minimum cracking energy of the Al 2024-T3 clad (h = 1.6 mm) is twice the value of thinner GLARE 3 (h = 1.37 mm). For low velocity loading (m_p = 2333 g), the minimum cracking energies of these materials are approximately equal; at high velocity the behavior of GLARE 3 is superior. This is caused by the influence of the strain rate on the strength of the glass fibre (Ref.18). Also 2024-T3 shows a different behaviour for static, low velocity and high velocity loading. This is consistent with other tests described in Ref.18. For 2024-T3 this is not caused by an increase of the strength of the material but it is caused by other dynamic effects, see table 1.

The minimum cracking energy of carbon/PEEK is equal for static, low and high velocity loading, and is low compared with Al 2024-T3 and GLARE. The minimum cracking energy of ARALL (aramid fibres) is in the same order as the thermoplastic composites, and is low compared with GLARE (glass fibres).

Dent depth

The dent depth for some of the materials is shown in Fig.5. The depth of the dent after impact is very small for the carbon/PEEK specimens (barely visible), and is approximately equal for GLARE 3 and Al 2024-T3. There is no difference between the dent depth of GLARE 3 at high and low velocity as is illustrated by the figure.

3. Impact tests on specimens under a tensile load

3.1 Introduction

The following objects may strike an aircraft structure under flight loads:
1. runway debris. This source of damage may strike lower wing structural parts under compressive loading.
2. hail and bird strike. Especially the front section of the fuselage (around the cockpit) may be hit in flight, while the fuselage is under cabin pressure.
3. ice from propellers and engine debris. Probably this will be the most serious threat for the fuselage structure under loading.
4. ballistic projectiles. Terrorist actions in the aircraft cabin may have catastrophic results. For military aircraft, ballistic impacts may hit every structural part under flight loads.

In this chapter instrumented impact tests are described on monolithic aluminium alloys and ARALL. A linear elastic model for sheet material impacted under a tensile load is derived.

3.2 Test set-up and materials

Fig. 6 shows the test set-up. The specimen dimensions were 300x160 mm², including the end-tabs for the grips of the 60 kN hydraulic testing machine. A specimen was loaded in the testing machine, and then clamped around a circular area with a diameter of 80 mm. Two plates clamped the specimen. The plates were firmly supported by braces attached to the hydraulic testing machine. This was done to assure well defined edge conditions of the tested area. The clamping

plates were supported to prevent the lateral displacements of the specimen with the clamping plates.

The circular clamped region of the specimen was struck in its centre by a pendulum: a weight of 689 g guided by strings attached to the top of the hydraulic testing machine. The impactor had a hemispherical steel nose with a radius of 7.5 mm. A stable swing of the pendulum was assured. The pendulum was instrumented: the contact force and the displacement were measured during impact and analyzed by computer.

The following materials were tested:
- 5 specimens of Al 2024-T3, h = 1.03 mm
- 5 specimens of Al 7075-T6, h = 1.03 mm
- 8 specimens of ARALL 2 (2/1 lay-up), h = 0.82 mm
- 3 specimens of ARALL 1 (2/1 lay-up), h = 0.82 mm

The specimens were tested in two ways:
1. 'Elastic' impact tests: very low impact energies, elastic deformation only. The specimens were tested at an impact energy of 0.13 J. These experiments were done for the verification of the model.
2. 'Plastic' impact tests: at higher energies, with plastic deformation. The impact energies are given in table 2.
The tensile stresses applied to the specimens before impact varied between S = 0 and S = 350 MPa, with a maximum value just below the yield stress of the material. After impact the crack length was measured.

3.3 Results and discussion

elastic impact tests
Fig.7 gives the results of the elastic impact tests on Al 2024-T3. Because the impact velocity showed some scatter for these tests with low velocities (0.6 m/s), the maximum force and the maximum central deflection during impact are divided by the impact velocity. The validity of this procedure will be shown in section 3.4.

The maximum central deflection and the contact time during impact decrease for an increasing preload, while the maximum force increases. The increase of the preload is audible: the frequency of the radiated sound during impact increases. The variation of the impact results is relatively small for the large range of the initial stress.

plastic impact tests
Figures 8 and 9 give typical examples of measured force-time and force-displacement curves during impact (no filtering was applied). Figure 8 illustrates that the dependence of the force-time curve on the preload stress level is small for monolithic material. The force-deflection curves show that the specimen tends to respond somewhat more stiffly as a result of the initial stress,

and the maximum force during impact is slightly higher.

The initial loading has more influence on the force-time and force-displacement curves of the ARALL material (Fig.9). This material shows cracking earlier in the deformation process for an increasing preload (see table 2).

The crack length as function of the initial stress is shown in Fig.10. In this figure the crack length at the impacted side (concave side) and the face opposite of the impacted side (convex side) are indicated. A significant rise of the crack length occurs at a relatively high prestress only: S > 150 MPa. This means that the effect will be small for operating stresses if S < 150 MPa. The change of the shape of the damage is important. Cracks in unstressed material branch and turn in fibre direction: a lip is formed in the material, and a hole is created. This will have a favourable influence on the stress concentration at the crack tip. The crack in prestressed material did not show this behaviour: the crack grows further in the direction perpendicular to the fibres and the loading. The stress concentration is not relieved, which will have a negative influence on the residual strength.

The results of the residual strength tests on ARALL 2 are shown in Fig.11. A large reduction of the residual strength was found for impact damage obtained under a preload stress S > 200 MPa.

3.4 Linear elastic analysis of impact on a clamped isotropic circular plate under initial tensile loading

As pointed out by Goldsmith (Ref.5), the simplest way to model the impacted specimen is by a mass-spring system. The clamped circular specimen is supposed to have a constant stiffness c and an equivalent mass m_{eq}. It is impacted by an impactor mass m_p with an impact velocity v_0. The following three assumptions are made:

1. Contact between the impactor and the plate is maintained during impact. Tests have shown that this is a reasonable assumption. In some cases only during the initial phase of the impact contact may be lost (In that case the plate is pushed away by the projectile, see Ref.18). The initial value of the velocity v_0^* of the mass-spring system at t=0 is derived from the conservation of momentum:

$$v_0^* = \frac{m_p}{m_p + m_{eq}} v_0 \qquad (1)$$

2. The stiffness of the system is practically equal to the static stiffness of the plate. For low velocities and a relatively large impactor mass the effect of stress waves and higher order vibrations in the plate may be neglected, and the deformation will be quasi-static. The stiffness is then supposed to be independent of the deflection, i.e. it is constant. This is a reasonable assumption for deflections smaller than the plate thickness. The stiffness is derived in Ref.18:

$$c = \frac{16\,\pi\,D}{a^2} = \frac{4\,\pi\,E\,h^3}{3(1-\nu^2)a^2} \qquad (2)$$

with: D as the flexural stiffness, diameter 2a, thickness h, material stiffness E, Poisson's ratio ν.

The equivalent mass of the specimen is derived in Ref.18 and is only a small fraction of the total mass of the plate (7/54 of the mass of the circular plate).

3. The kinetic energy of the impactor is fully transferred to kinetic energy of the impactor and the plate, and to internal strain energy of the plate. Higher order vibrations of the plate, the energy spent for local Hertzian indentation and the deformation of the clamping and impactor are neglected. Also the change of potential energy (the influence of gravity) is ignored. Higher order vibrations will have little effect for high impactor masses relative to the equivalent plate mass, as is the case in our tests.

With the above assumptions the impact problem can be reduced to its simplest form:

$$m_{tot}\,\ddot{w}_0 + c\,w_0 = 0 \qquad (3)$$

with $m_{tot} = m_{eq} + m_p$, and w_o as the central deflection of the plate.

The solution of Eq.3 for the central deflection, the velocity, the contact force and the contact time is:

$$w_{r=0} = v^{\bullet}_{t=0} \sqrt{\frac{m_{tot}}{c}} \sin\left[\sqrt{\frac{c}{m_{tot}}}\, t\right]$$

$$v = v^{\bullet}_{t=0} \cos\left[\sqrt{\frac{c}{m_{tot}}}\, t\right]$$

$$F = v^{\bullet}_{t=0}\, m_p \sqrt{\frac{c}{m_{tot}}} \sin\left[\sqrt{\frac{c}{m_{tot}}}\, t\right] \qquad (4)$$

$$t_c = \pi \sqrt{\frac{m_{tot}}{c}}$$

The contact time t_c is the time at $F = 0$, after initial contact. The contact time is independent of the impact velocity.

A preload N_x per unit of length is present in the x-direction of the circular plate. According to Timoshenko and Woinowsky-Krieger (Ref.15) the strain energy during bending of the plate will be increased with:

$$U_s = \frac{1}{2} \iint_{Area} N_x \left(\frac{\delta w}{\delta x}\right)^2 dx\, dy \qquad (5)$$

This equation 5 was integrated with the deflection shape of a centrally loaded circular clamped plate:

$$w = w_0 \left[1 + \left(\frac{r}{a} \right)^2 \left(2 \ln \left(\frac{r}{a} \right) - 1 \right) \right] \qquad (6)$$

The internal strain energy due to an intial stress S can be calculated by substitution of Eq.6 in Eq.5:

$$U_s = \frac{1}{4} \pi S h w_0^2 \qquad (7)$$

This energy is not dependent on the size of the clamped area of the plate. It means that the effective stiffness of the plate will be increased by the initial stress with:

$$\Delta c = \frac{1}{2} \pi S h \qquad (8)$$

Equations (4) can still be used. The additional stiffness, due to the initial loading has to be taken into account by substitution of the total stiffness $c_{tot} = c + \Delta c$.

The extended model was compared with the experimental results. The stiffness of the Al 2024-T3 specimen (h = 1.0 mm, clamped area diameter 2a = 80 mm) is c = 212 N/mm. The additional stiffness Δc at an initial stress of 300 MPa is 471 N/mm, which is a significant stiffness increase. The equivalent mass of the specimen is 2 g. This mass is small relative to the impactor mass. In Fig.7 the extended mass-spring model is compared with the experimental results. The results of the model agree well with the measured values. The maximum force during impact increases and the maximum central deflection decreases with increasing initial load. The contact time becomes shorter.

3.5 Ballistic impact tests

The testing device shown in Fig.12 was used to study the behaviour of GLARE 3 (t = 1.4 mm, GLARE fuselage design) and Al 2024-T3 clad (t = 1.6 mm, conventional fuselage design Airbus A340) under biaxial loading as is realistic for engine fragments hitting an aircraft fuselage. A fragment simulating projectile (Fig. 13) with a diameter of 20 mm and a mass of 54 g was shot with a velocity of 400 m/s through the centre of the specimen. The width of the specimen at the load introduction was 160 mm; the loaded specimens were biaxially loaded with a load of 35 kN. This results in a biaxial stress field of 137 MPa for 2024-T3 and 156 MPa for GLARE 3. The homogenety and the intensity of the stress field was checked with strain gage measurements. One unloaded Al 2024-T3 and two unloaded GLARE 3 and two biaxially loaded 2024-T3 and three biaxially loaded GLARE 3 specimens were tested. After the ballistic tests the specimens were cut to a rectangular specimen with a width of 160 mm and pulled to failure under static loading.

Fig. 14 shows that a lot af damage is created at the back (projectile exit) side of the GLARE specimens. The fragment peels of the thin aluminium layer at the back side of the laminate. No effect of the biaxial loading on the size of the damage was observed. Although the damage size in GLARE is greater than in 2024-T3, the residual load carrying capability of both materials is similar, as is shown in Fig. 15.

4. Conclusions

Comparison of static loading, low velocity and high velocity impact.

1. The minimum cracking energy of GLARE 3 and Al 2024-T3 increases with a higher rate of loading. For GLARE 3 this effect is more pronounced than for Al 2024-T3 because of the strain rate dependent behaviour of the glass fibre. The minimum cracking energy of carbon/PEEK for static, low velocity and high velocity loading is equally low.

2. The dent depth after impact of carbon/PEEK, GLARE 3 and Al 2024-T3 is not affected by the velocity of impact; instead, it only varies as a function of impact energy.

3. No influence was found of the loading rate (low and high velocity) on the damage width of GLARE.

Comparison of damage resistance of the different materials

1. GLARE 3 has a smaller damage size than carbon/PEEK with the same thickness or with the same areal density.

2. GLARE 3 has the highest minimum cracking energy compared with monolithic aluminium, ARALL and carbon/PEEK with the same areal density (see figure 4).

3. GLARE 3 (h = 1.37 mm) has a lower minimum cracking energy than the heavier baseline Al 2024-T3 clad (h = 1.6 mm) material under static loading, approximately an equal minimum cracking energy in low velocity impact and a superior behavior in high velocity impact loading (see figure 4).

4. The depth of the dent after impact for GLARE 3 is approximately equal to Al 2024-T3 (h = 1.37 and 1.6 mm). This makes the detection of impact damage easy.

Effect of tensile loading

1. The length of a crack caused by impact on ARALL loaded in tension increases for an increasing preload tension stress S (Fig.10). A significant increase of the crack length will occur only for a relatively high preload stress (S > 150 MPa).

2. The shape of the damage in ARALL is changed by the preload. There is no longer a tendency for the crack to bend in fibre direction to form a lip and to create a hole. The crack remains in the direction perpendicular to the loading. This will increase the stress concentration and reduce residual strength.

3. If extensive cracking during impact of a preloaded specimen does not occur, a higher contact force during impact and a smaller maximum central deflection are observed. The influence of the preload on the maximum contact force and the maximum central deflection was rather small. These trends can be described by an elastic impact model.

4. GLARE shows significantly more damage after ballistic impact of fragment simulating projectiles, but this damage is primarily present in the outer aluminium layer at the exit side of the projectile. The residual load carrying capability of GLARE (thickness of 1.37 mm, areal density 3.41 kg/m^2) is in this case equal to Al 2024-T3 (thickness 1.6 mm, areal density 4.45 kg/m^2.

Acknowledgement

Research is teamwork. The research described in this article was supported in many ways by professor J. Schijve, professor L.B. Vogelesang, Captain Robert Fredell, USAF, Peter Bulters and Anne Oldersma.

References

1. Awerbuch, J.; Impact damage in composite materials, Composite materials workshop, Katholieke Universiteit, Leuven, 1984.
2. Card, M.F.; Rhodes, M.D.; Effect of service environment on composite materials, AGARD 50th Meeting on the structures and materials panel specialists meeting, 1980.
3. Elber, W.; The effect of matrix and fibre properties on impact resistance, in: Tough composite materials, NASA CP 2334, pp.99-121, 1983.

4. Gökgöl, O.; A310-300 CFRP fin damage tolerance demonstration, 7th International SAMPE conference, Munich, 1986.
5. Goldsmith, W.; Impact, the theory and physical behaviour of colliding solids, London, 1960.
6. Gunnink, J.W.; Vogelesang, L.B.; Aerospace ARALL, The advancement in aircraft materials, Proceedings 35th International SAMPE symposium, Anaheim, California, April 2-5, 1990.
7. Hart, W.G.J. 't; Frijns, R.H.W.M.; Damage tolerance properties of new carbon composites, NLR Technical Publication TP 89032 L, 1989.
8. Hart, W.G.J. 't; Frijns, R.H.W.M.; Delamination growth in improved carbon composites under constant amplitude fatigue loading, NLR Technical Publication TP 89008 L, 1989.
9. Oplinger, D.W.;Slepetz,J.M.;Impact damage tolerance of Graphite/Epoxy sandwich panels, in: Foreign object impact damage to composites, ASTM STP 568, 1975.
10. Roebroeks, G.H.J.J.; Towards GLARE - The development of a fatigue insensitive and damage tolerant material, PhD thesis Delft University of Technology, 1991.
11. Sankar, B.V.; Sun, C.T.; Low velocity impact damage in graphite-epoxy laminates subjected to tensile initial stresses, AIAA Journal Vol.24, No.3, 1986.
12. Shivakumar, K.N.; Elber, W.; Illg, W.; Prediction of low-velocity impact damage in thin circular laminates, AIAA Journal, Vol.23, No.3, pp.442-449, 1985.
13. Suarez, J.A. ; Whiteside, J.B.; Comparison of residual strength of composite and metal structures after ballistic damage, in: Foreign object impact damage to composites, ASTM STP 568, 1975.
14. Sun, C.T.; Chen, J.K.; On the impact of initially stressed composite laminates, J.Composite materials, Vol.19, pp.490-504, 1985.
15. Timoshenko, S.P.; Woinowsky-Krieger, S.; Theory of plates and shells; McGraw-Hill Book Company, 1970.
16. Vogelesang, L.B.; Gunnink, J.W.; ARALL, a material for the nextgeneration of aircraft, TU Delft report LR400, Delft, 1983.
17. Vogelesang, L.B.; Gunnink, J.W.; ARALL; a materials challenge for the next generation of aircraft, Materials and design, Vol.7, No.6, 1986.
18. Vlot, A.; Low-velocity impact loading on fibre reinforced aluminium laminates (ARALL) and other aircraft sheet materials, PhD thesis Delft University of Technology, 1991.
19. Vlot, A.; Bulters, B.M.; Fredell, R.S.; Low and high velocity impact loading on fibre/metal lainates, carbon/PEEK and monolithic aluminium 2024-T3, Proceedings of the 13th International European Chapter Conference of the Society for the Advancement of Material and Process Engeineering, Hamburg, Germany, May 11-13, 1992.
20. Wu, H.T.; Springer, G.S.; Impact induced stresses, strainsand delaminations in composite plates, J.Composite materials, Vol.22, pp.533-560, 1988.
21. Zukas, J.A.; Nicholas, T.; Swift, H.; Greszcuk, L.B.; Curran, D.R.; Impact Dynamics, John Wiley & Sons, 1982.
22. Bulters, P.B.M.; Static and Ballistic Impact Tests on Biaxial Loaded cruciform

Shaped Specimen, Thesis TU Delft, 1991.
23. Fredell, R.; Vlot, A.; Verbruggen, M.; Fatigue and Residual Strength Characteristics of Fiber Metal Laminates Subjected to Incidental Damage, TU Delft report LR-708, 1992.
24. Fredell, R.; The Development of Inspection and Repair Methods for the C-17 Aft Cargo Door, TU Delft report LR-704, 1992.

material	h (mm)	strain rate (s^{-1})	ultimate tensile stress (MPa)
7075-T6	1.55	$4\ 10^{-4}$	593
		3.5	546
		35	548
GLARE 3 (based on Al 7075-T6)	1.35	$4\ 10^{-4}$	666
		3.8	753
		38	803
		69	832

table 1 Results of high strain rate tensile tests (Ref.18).

material	initial stress	impact energy	max. during impact F_{max}	max. during impact w_o	contact time	crack length convex	crack length concave
	(MPa)	(J)	(kN)	(mm)	(ms)	(mm)	(mm)
2024-T3	0	4.74	1.87	5.32	3.03	0	0
	200	4.74	2.07	4.77	3.17	0	0
	350	4.74	1.84	4.69	2.77	0	0
	350	4.74	2.09	5.03	3.10	0	0
	350	6.80	1.78	5.96	3.03	0	0
7075-T6	0	7.32	2.80	6.52	2.53	0	0
	100	7.32	2.86	5.61	2.83	0	0
	200	7.32	3.08	4.20	2.57	0	0
	300	7.32	2.80	6.52	2.53	0	0
	300	7.32	2.64	4.51	-	0	0
2H32	0	6.12	2.21	-	-	7.9	0
	0	6.12	2.40	6.08	3.17	7.2	0
	100	6.12	2.37	5.54	4.36	7.7	0
	200	6.12	1.95	5.66	-	12.8	12.5
	300	6.12	1.95	5.50	4.69	20.9	19.1
	100	9.39	2.03	8.36	3.95	10.7	8.7
	200	9.39	2.26	12.5	3.90	12.8	12.5
	300	9.39	1.68	10.4	7.19	failure	
7H32	0	6.12	2.53	5.78	3.60	8.5	0
	150	6.12	2.33	5.42	2.93	9.7	0
	250	6.12	2.36	5.38	5.00	27.8	27.2

table 2 Results of the plastic impact tests (2H32 = ARALL 2, 7H32 = ARALL 1).

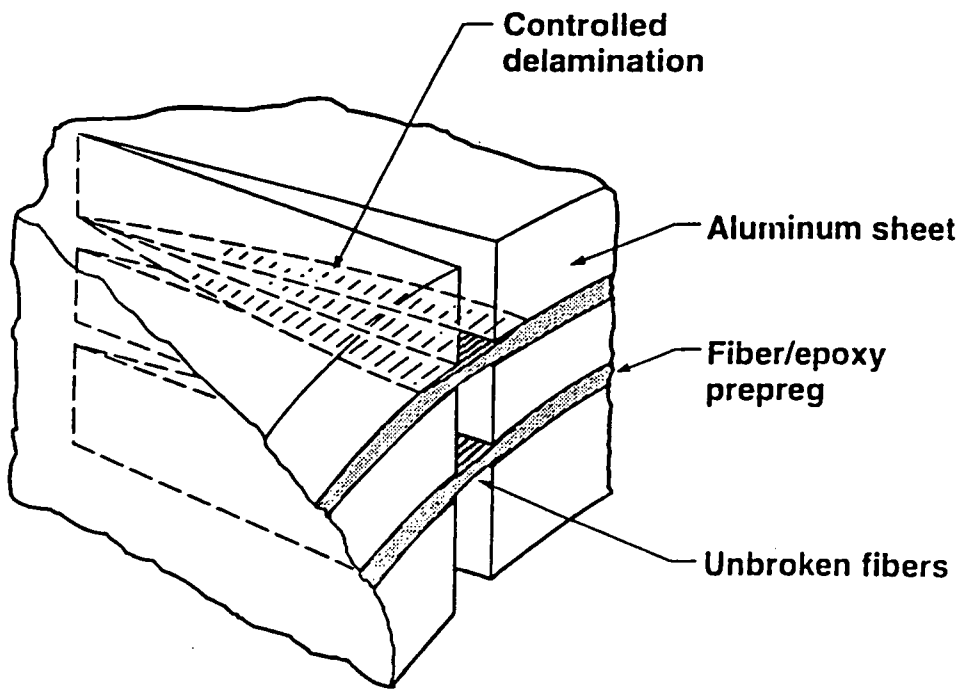

figure 1 Schematic showing crack bridging by intact fibres in crack wake.

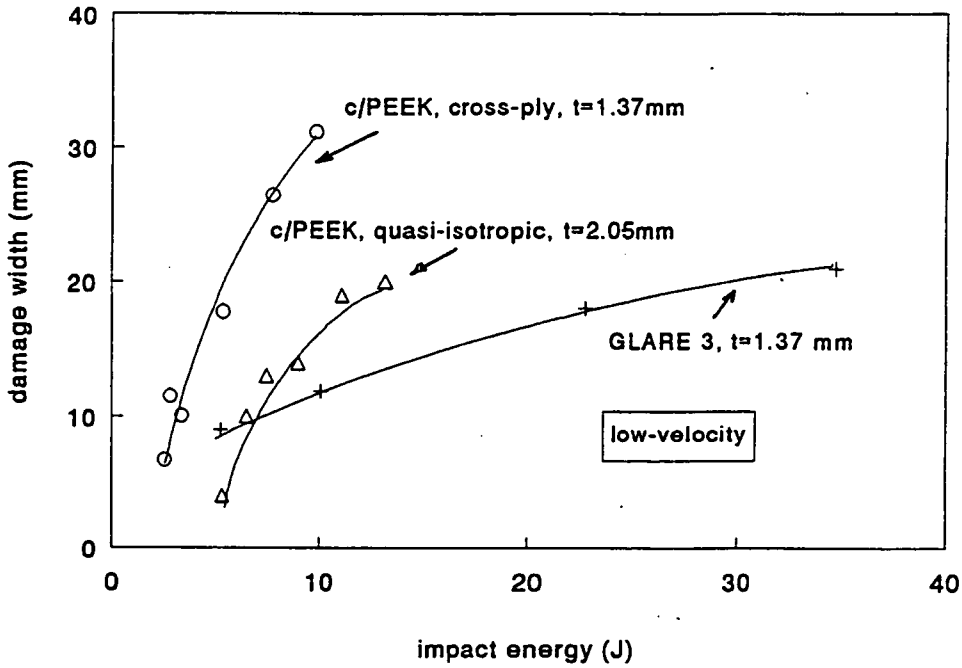

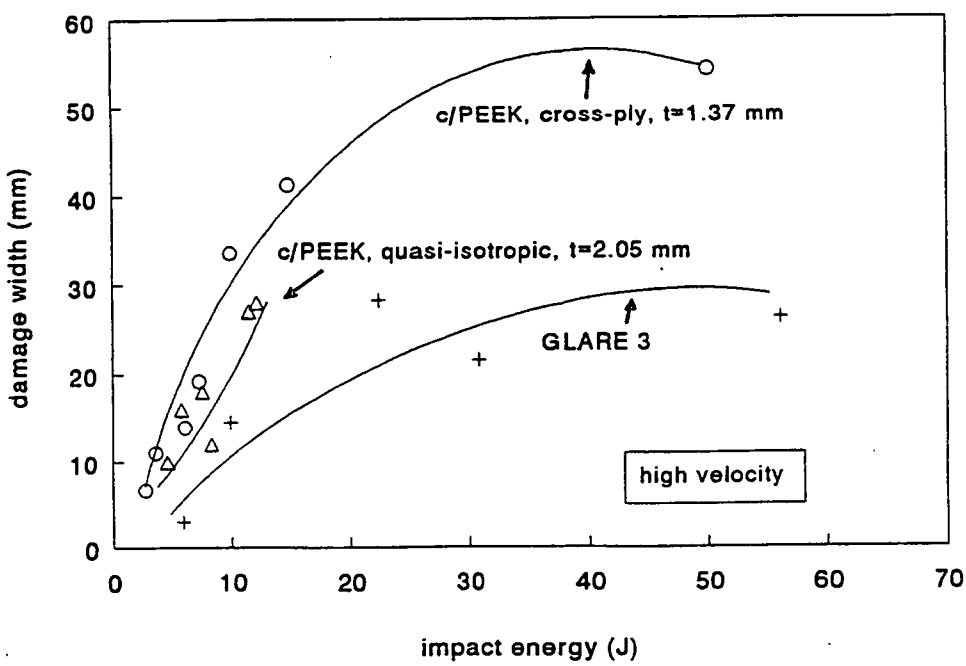

figure 2 The damage width as function of the impact energy.

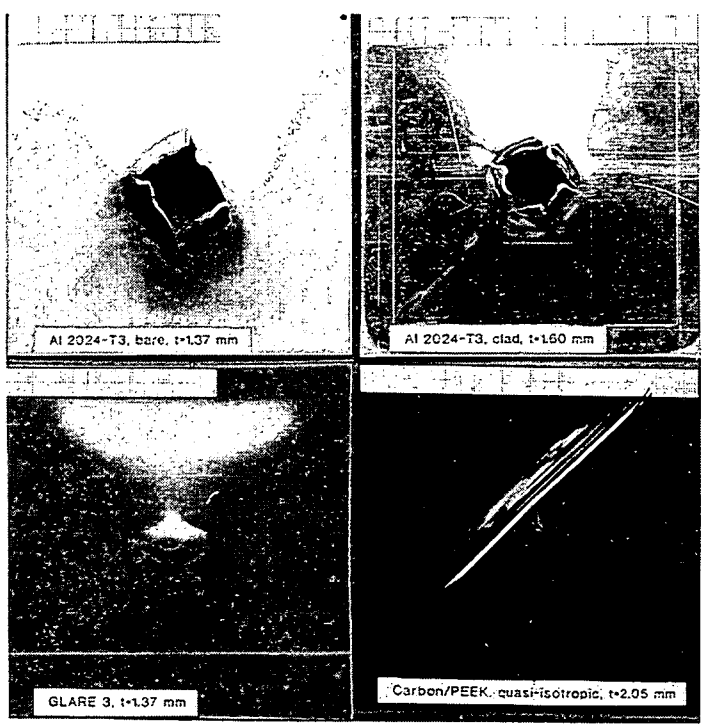

figure 3 Specimens after high velocity impact at approximately 100 J (back face). Perforation of the projectile in aluminium and carbon/PEEK, minor crack in GLARE-3 in outer layer only.

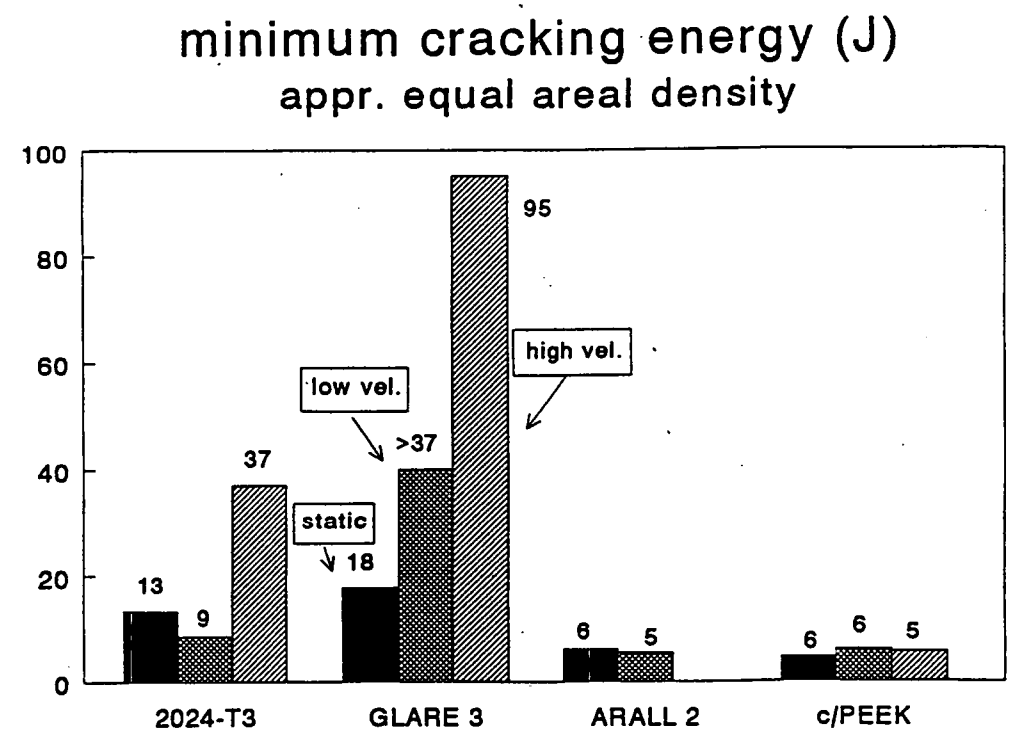

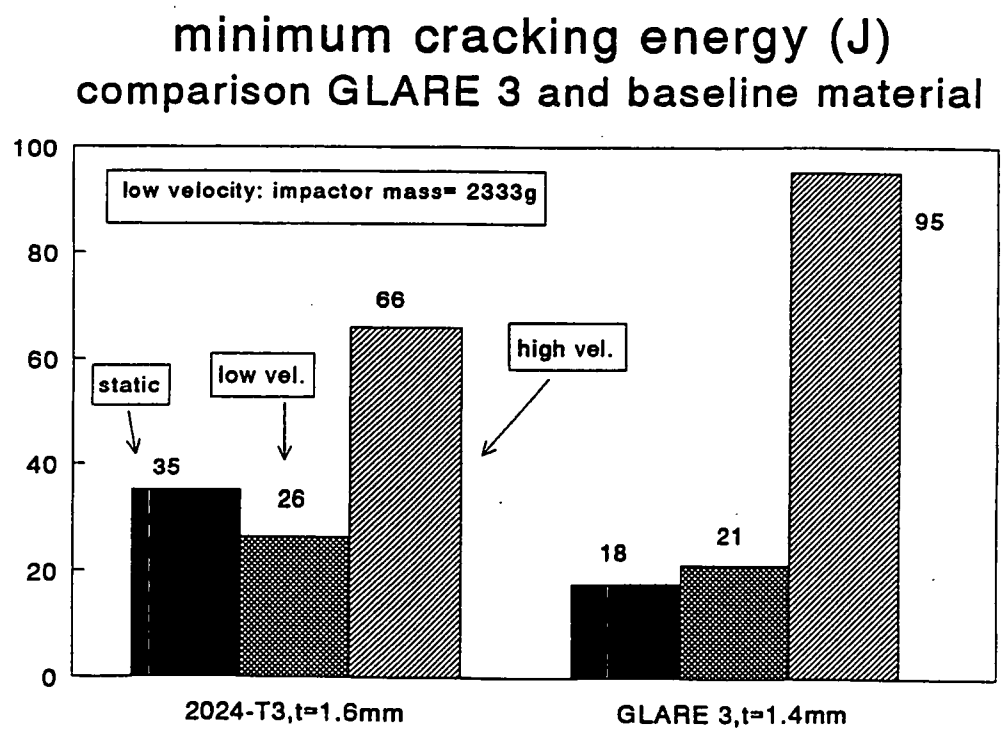

figure 4 A comparison of the minimum cracking energy of the materials.

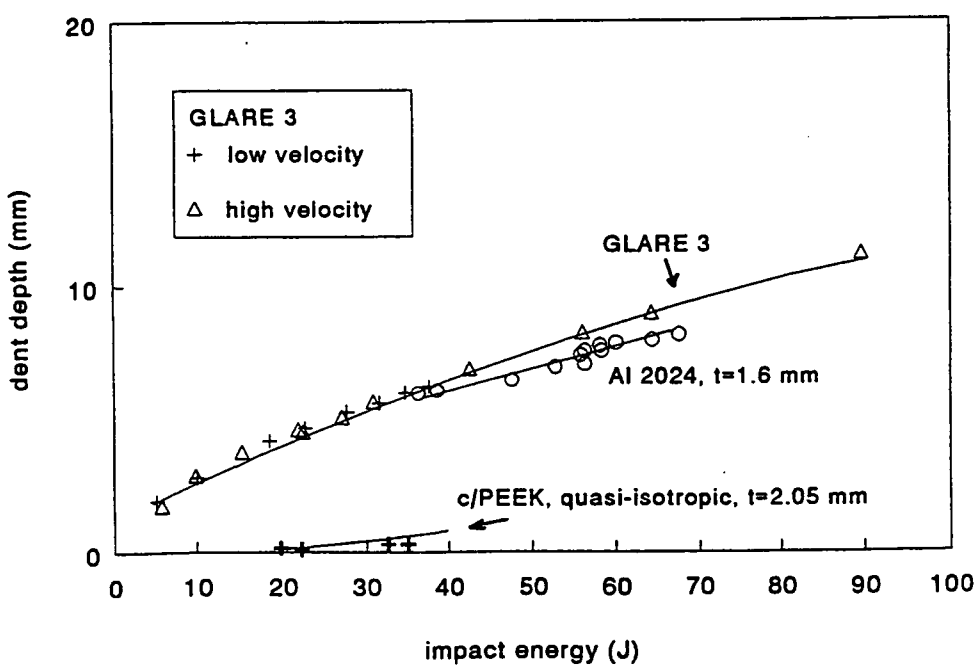

figure 5 The depth of the dent after impact as function of the impact energy (Al 2024 and c/PEEK: high velocity).

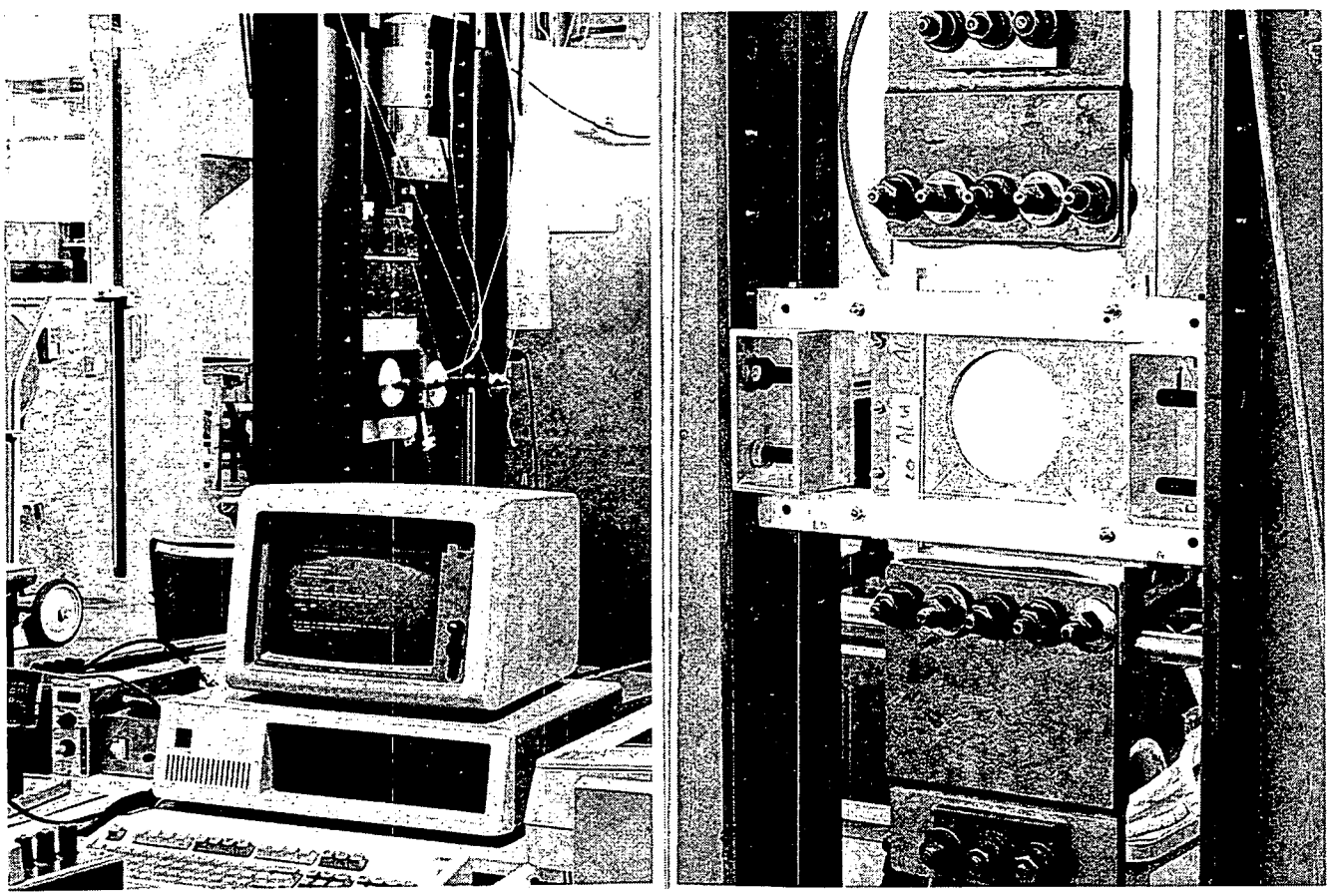

figure 6 Test set-up for impact tests on specimens under initial tensile load.

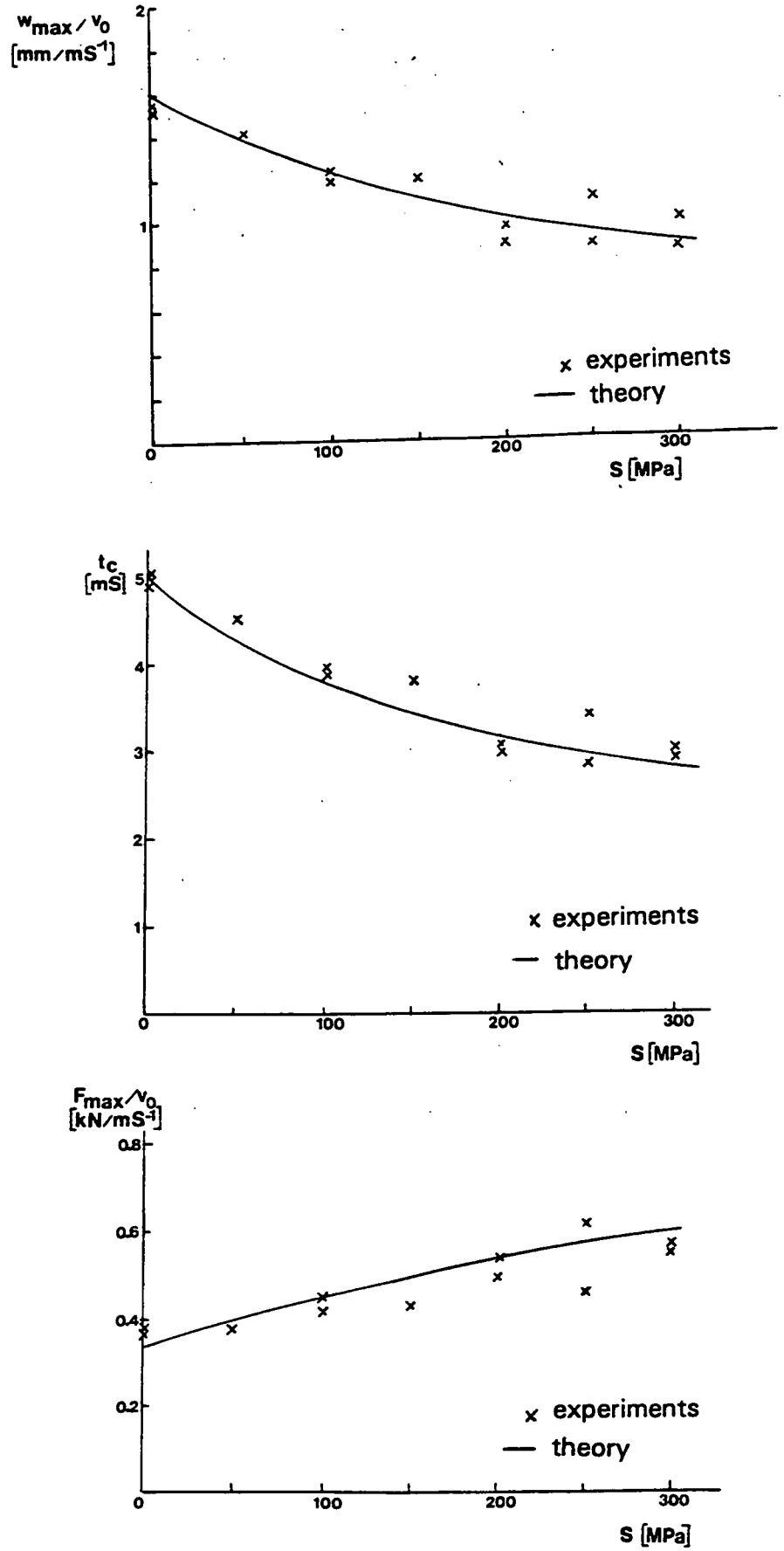

figure 7 Results of elastic impact tests on Al 2024-T3 (h = 1.0 mm), comparison of test results and model.

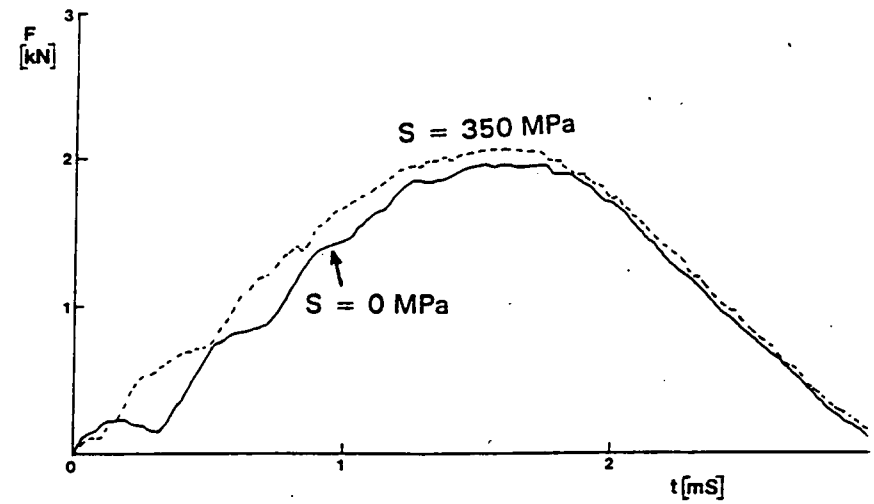

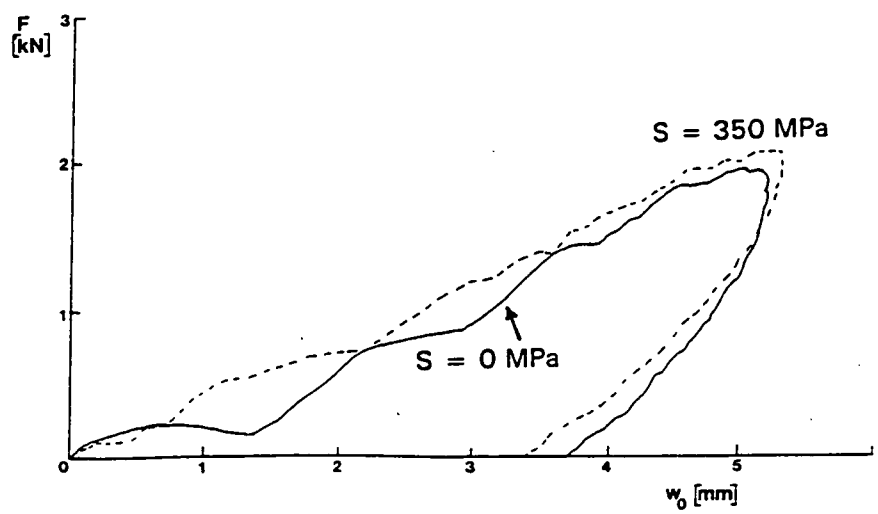

figure 8 Typical force-time and force-deflection curves for Al 2024-T3 (h = 1.0 mm) at an impact energy of 4.74 J.

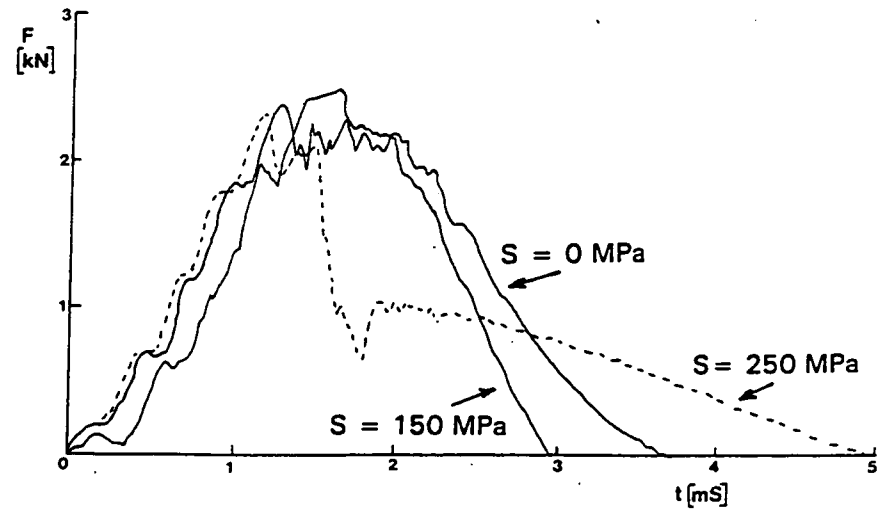

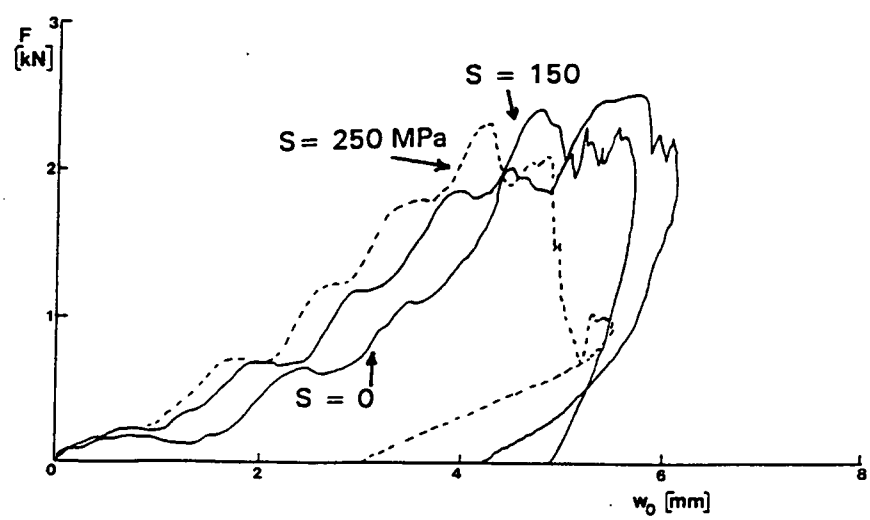

figure 9 Typical force-time and force-deflection curves for ARALL 1 (h = 0.8 mm) at an impact energy of 6.12 J.

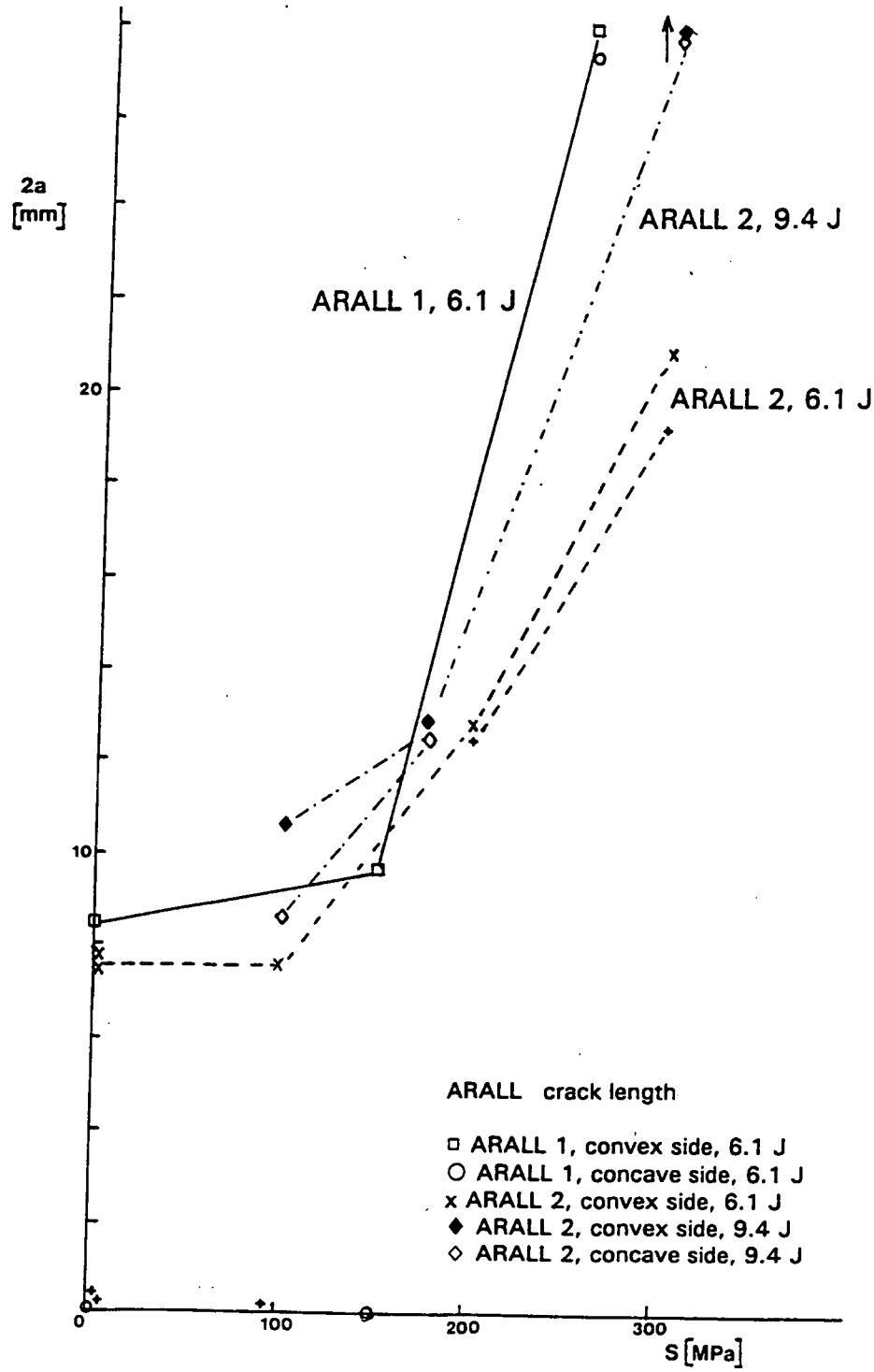

figure 10 The total crack length after impact as function of the initial stress.

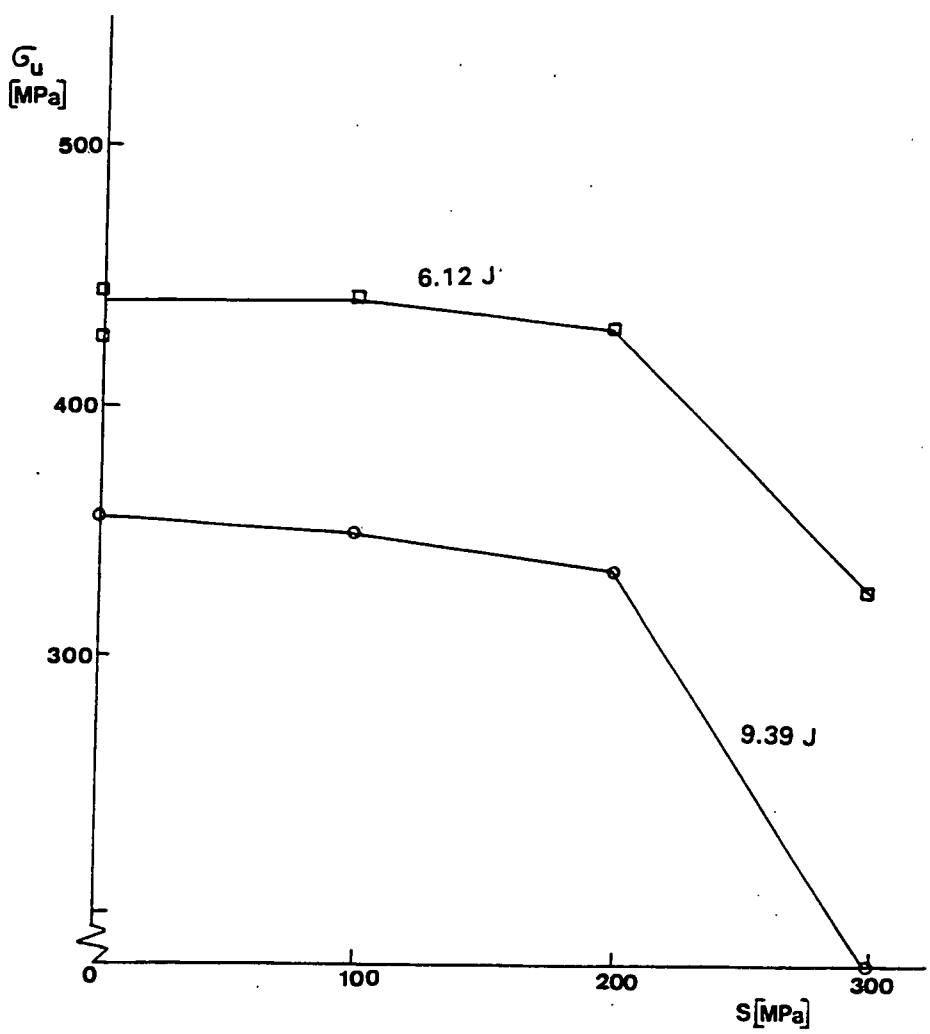

figure 11 The residual strength as function of the intial stress for ARALL 2.

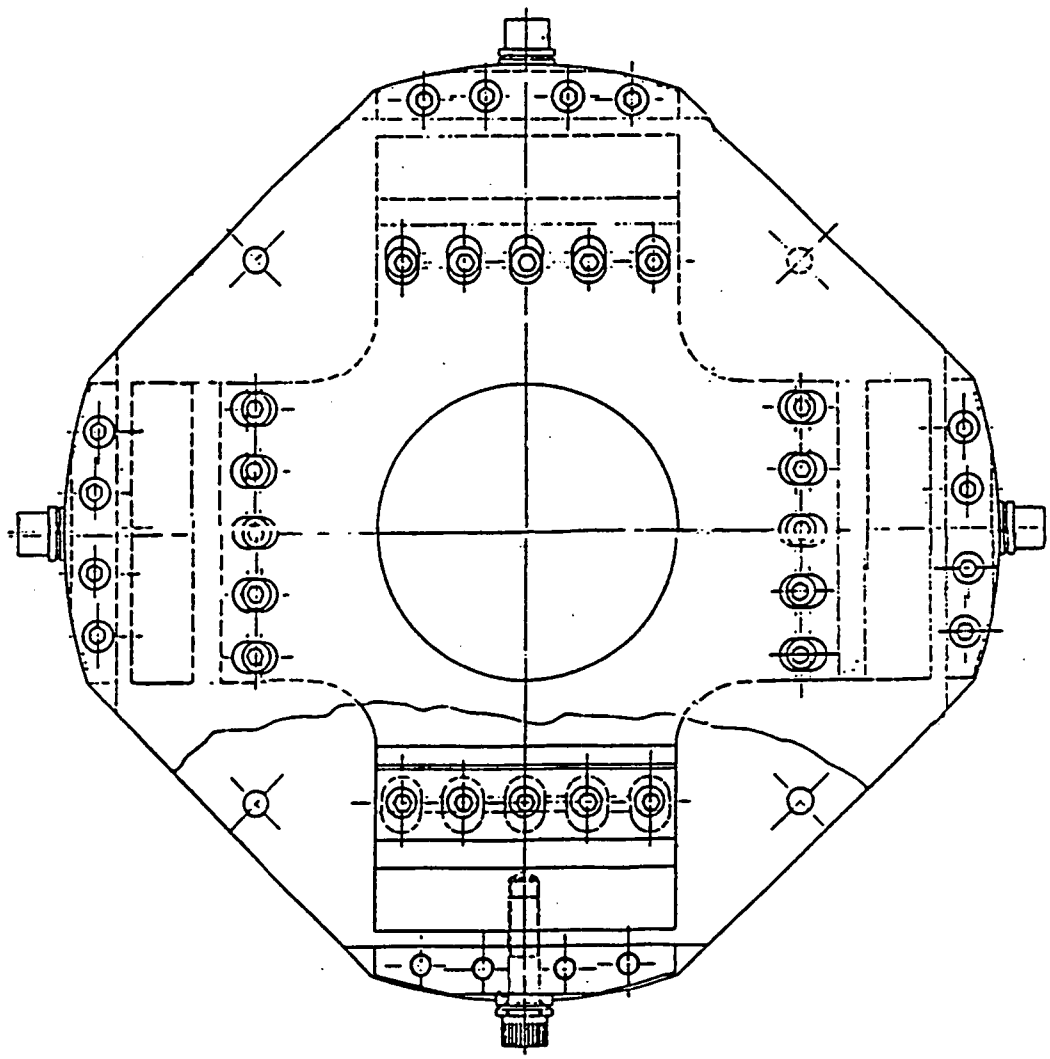

figure 12 Clamping device to introduce biaxial loading for ballistic impact tests.

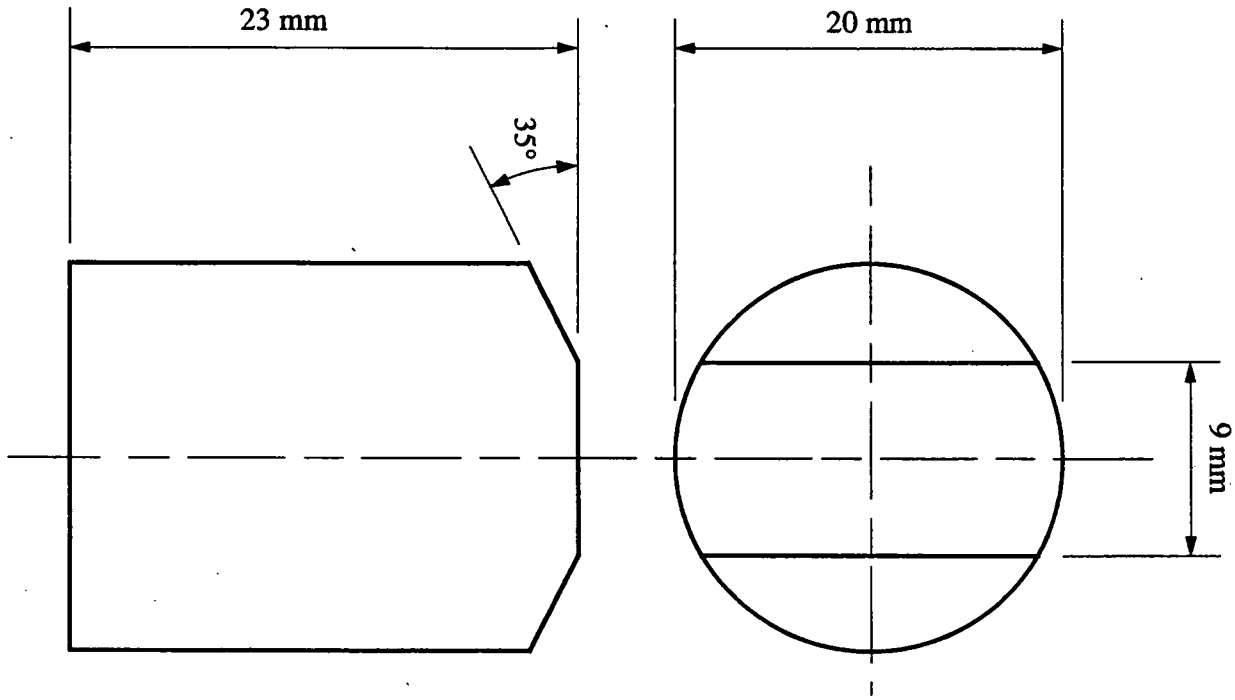

figure 13 Fragment simulating projectile.

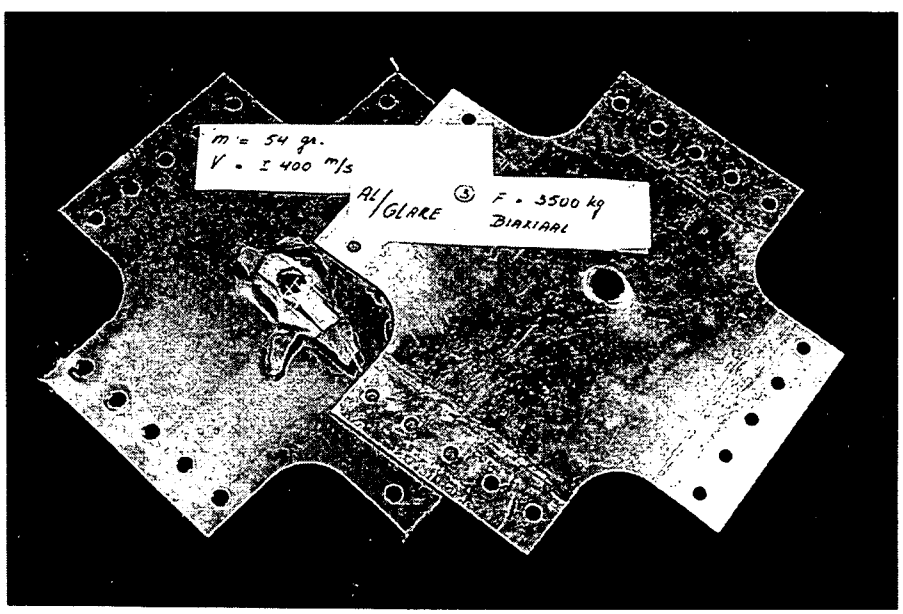

Figure 14 GLARE and aluminium specimens after ballistic impact (exit side).

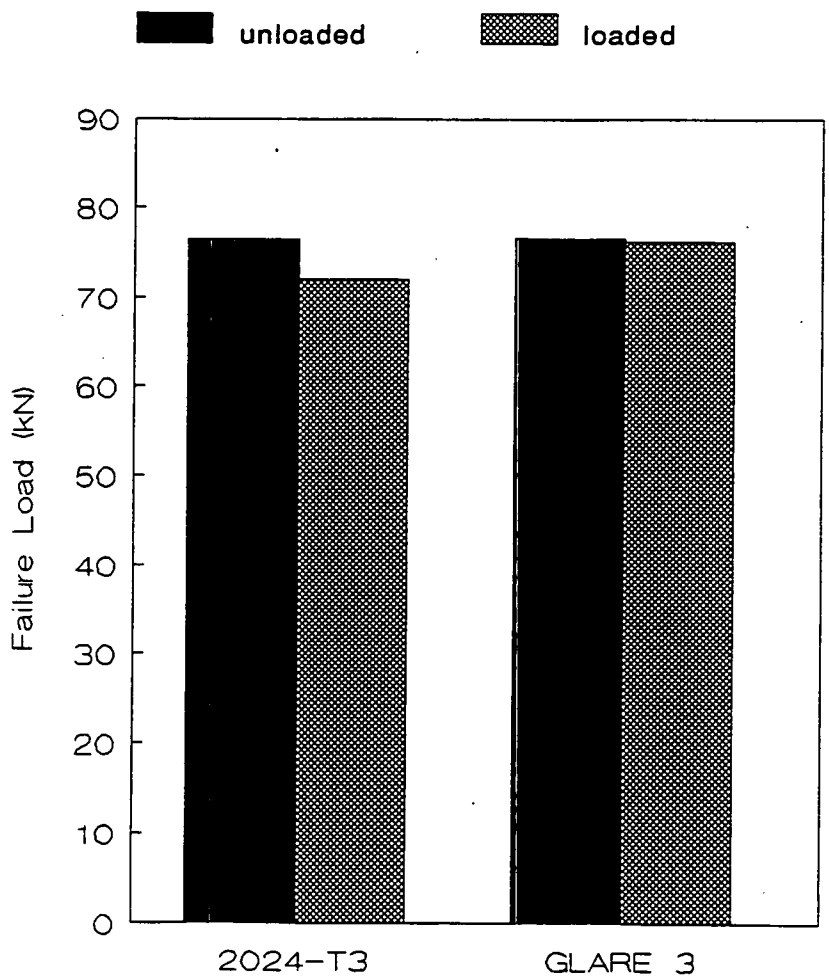

figure 15 Failure loads during residual strength tests after ballistic impact.